Table II. Activation Energy for Grain-Boundary Mobility of Polycrystalline Y_2O_3

Ionic species	Annealing atmosphere	Activation energy (kJ/mol)	Temperature (°C)	Reference
?	In vacuum	340	1500–1700	Sordelet and Akinc[36]
Y	In air	399	1500–1650	Chen and Chen[24]

?Unidentified.

diffusion is significantly lower than that for yttrium cation's diffusion. The activation energy of the grain-boundary migration in the present study is lower than that of the diffusion coefficient of yttrium cation, and is close to that of the oxygen anion's lattice diffusion.[39] However, yttrium cation should be the rate-controlling species for lattice diffusion in Y_2O_3, because the yttrium cation's lattice diffusion is much slower than the oxygen anion's lattice diffusion.[18,27]

When the grain growth during SPS is controlled by lattice diffusion, there are two possible explanations for the low activation energy for the grain-boundary migration. (1) The activation energy corresponds to that for oxygen lattice diffusion and the rate-controlling species is oxygen anion; the diffusion of yttrium cation is accelerated by SPS and becomes faster than the diffusion of oxygen anion. (2) The activation energy for the grain growth corresponds to that for the diffusion of yttrium cation; the diffusion of yttrium cation is rate-controlling. In both cases, the diffusion of yttrium cation should be accelerated by SPS.

When the grain-boundary migration during SPS is controlled by grain-boundary diffusion, the low activation energy observed in the present study must correspond to that for the grain-boundary diffusion of Y_2O_3 accelerated by SPS. There have been earlier studies reporting that high-temperature matter transport in fine-grained Y_2O_3 mainly occurs by grain-boundary diffusion. Wang *et al.*[41] showed that during two-step sintering, grain growth to a final size of 400 nm proceeds by grain-boundary diffusion. They also indicated that grain-boundary migration in Y_2O_3 is rate-controlled by grain-boundary diffusion of yttrium cation.[24] In addition, our recent study[42,43] concerning the influence of cation-doping on the sintering of Y_2O_3 suggests that densification in Y_2O_3 with a grain size of <2 μm mainly occurs by grain-boundary diffusion. These studies strongly support the idea that in the fine-grained Y_2O_3 used the present study, grain-boundary migration during SPS is also controlled by grain-boundary diffusion. Although the rate-controlling species and diffusion path cannot be determined by the present study, the above discussion strongly suggests that diffusion of yttrium cation in Y_2O_3 is accelerated by SPS.

(3) Defect Chemistry During SPS

The present EELS result supports the fact that the formation of atomic defects is involved in the grain boundaries of Y_2O_3 by SPS. Because an electric field and compressive stress during SPS must mainly influence particle surface and grain boundary of materials, it is reasonable that the formation of atomic defects is prominent at grain boundary in comparison with grain interior. It has been reported that O-*K* ELNES in Y_2O_3 depends on oxygen stoichiometry[26]; the intensity of peak α is lower/higher than that of peak β in stoichiometric/reduced Y_2O_3 powders prepared by electron beam irradiation, and the chemical shift is explained from the presence of oxygen anion vacancies. The chemical shift observed in the present study is opposite to previous data, but the inconsistency probably results from difference in the sample preparation methods and/or from the presence of interstitial yttrium cations.

Table III. Activation Energy for Diffusion Coefficient of Y_2O_3

Sample	Ionic species	Activation energy (kJ/mol)	Reference
Single crystal	O	82	Berard *et al.*[37]
Single crystal	O	191	Ando *et al.*[39]
Single crystal	Y	301	Gaboriaud[38]
Dense polycrystal	Y	290	Berard and Wilder[40]
Polycrystal	Y	410	Wang *et al.*[41]

It has been reported that grain growth in Y_2O_3 is rate-controlled by Y^{3+} diffusion via the cation interstitial mechanism[24]; the grain-boundary mobility was reported to be higher in a reducing atmosphere than in air.[24] The following defect reactions perhaps take place under reduced pressure.

$$O_O \leftrightarrow V_O^{\bullet\bullet} + 2e' + \frac{1}{2}O_2 \tag{2}$$

$$3V_O^{\bullet\bullet} + 2Y_Y \rightarrow 2Y_i^{\bullet\bullet\bullet} \tag{3}$$

where O_O indicates an oxygen anion on an oxygen anion site in Y_2O_3, $V_O^{\bullet\bullet}$ is a vacant oxygen anion with a double positive effective charge relative to the perfect Y_2O_3 lattice, e' is an electron with a negative charge, Y_Y is a yttrium cation on a yttrium site in Y_2O_3, and $Y_i^{\bullet\bullet\bullet}$ is an interstitial yttrium cation with an excess+3 charge. It is possible that an electric field applied during SPS enhances the above defect reaction that involves an electron emission. The SPS may activate the formation of oxygen vacancies and interstitial yttrium cations, and consequently enhance matter transport in Y_2O_3. Although a first-principle calculation is necessary to interpret the ELNES data, the chemical shift observed in the grain boundary of the SPSed Y_2O_3 must represent the formation of atomic defects involved in the SPS. The improved sinterability and accelerated grain-boundary migration in Y_2O_3 is attributed to the enhanced diffusion that arises from the defect formation activated by SPS.

V. Conclusions

The sinterability of nanocrystalline Y_2O_3 was investigated by SPS for a combination of low sintering temperatures (850°–1050°C) and low heating rates (2–50°C/min). For elucidation of the mechanism of the low-temperature densification of Y_2O_3 by SPS, the microstructure of the sintered materials was investigated by HRTEM, EDS and EELS. The results are summarized as follows:

(1) Translucent polycrystalline Y_2O_3 with a relative density of 99% was obtained by SPS at a sintering temperature of 950° or 1050°C and a heating rate of 2°C/min. The sintering temperature is significantly lower than that required for the fabrication of dense Y_2O_3 by pressureless sintering.

(2) At a sintering temperature of 950°C and a heating rate of 2°C/min, the SPS yielded Y_2O_3 with the relative density of 99% and the average grain size of 190 nm. Lower heating rates result in higher relative densities and smaller grain sizes in the SPS.

(3) The isothermal SPS experiment indicated that the grain-boundary mobility is highly enhanced by the SPS in comparison with the pressureless sintering; the grain-boundary mobility at 950°C was comparable to the previously reported data for Y_2O_3 by pressureless annealing at around 1500°C in air.

(4) The HRTEM observation revealed that the Y_2O_3 sintered by SPS exhibits a single-phase microstructure without a grain-boundary amorphous layer. In addition, no impurity incorporation was detected by the nanoprobe EDS analysis. The improved sinterability and enhanced grain-boundary mobility are attributed to neither liquid-phase sintering nor impurity effects.

(5) The EELS analysis indicated that the SPS changes the atomic configuration of the grain boundaries. The improved sinterability and accelerated grain-boundary mobility is attributed to the defect formation activated by the SPS.

References

[1]Y. Tsukuda, "Application for Refractory and Corrosion Resistant Materials," *Jpn. Ceram. Soc. Bull.*, **23** [5] 456–60 (1988).

[2]C. E. Curtis, "Properties of Yttrium Oxide Ceramics," *J. Am. Ceram. Soc.*, **40** [8] 274–8 (1957).

[3]K. A. Wickersheim and R. A. Lefever, "Infrared Transmittance of Crystalline Yttrium Oxide and Related Compounds," *J. Electrochem. Soc.*, **111** [1] 47–51 (1964).

[4]C. Brecher, G. C. Wei, and W. H. Rhodes, "Point Defects in Optical Ceramics: High-Temperature Absorption Processes in Lanthana-Strengthened Yttria," *J. Am. Ceram. Soc.*, **73** [6] 1473–88 (1990).

[5]M. Foex, "Research on the Melting Point of Yttrium Oxide," *High Temp.-High Press.*, **9** [3] 269–82 (1977).

[6]T. Yamada, M. Yoshimura, and S. Somiya, "Redetermination of the Solidification Points of Al_2O_3, Y_2O_3, and HfO_2 by Digital Pyrometry with an Arc-Imaging Furnace," *High Temp.-High Press.*, **18** [4] 377–88 (1986).

[7]R. A. Lefever and J. Matsko, "Transparent Yttrium Oxide Ceramics," *Mat. Res. Bull.*, **2**, 865–9 (1967).

[8]K. Majima, N. Niimi, M. Watanabe, S. Katsuyama, and H. Nagai, "Effect of LiF Addition on the Preparation of Transparent Y_2O_3 by the Vacuum Hot Pressing Method," *J. Alloys Compd.*, **193**, 280–2 (1993).

[9]S. K. Dutta and G. E. Gazza, "Transparent Y_2O_3 by Hot-Pressing," *Mat. Res. Bull.*, **4**, 791–6 (1969).

[10]J. Zhang, S. Wang, L. An, M. Liu, and L. Chen, "Infrared to Visible Upconversion Luminescence in $Eu^{3+}Y_2O_3$ Transparent Ceramics," *J. Lumin.*, **122–123**, 8–10 (2007).

[11]N. Saito, S. Matsuda, and T. Ikegami, "Fabrication of Transparent Yttria Ceramics at Low Temperature Using Carbonate-Derived Powder," *J. Am. Ceram. Soc.*, **81** [8] 2023–8 (1998).

[12]T. Ikegami, J.-G. Li, T. Mori, and Y. Moriyoshi, "Fabrication of Transparent Yttria Ceramics by the Low-Temperature Synthesis of Yttrium Hydroxide," *J. Am. Ceram. Soc.*, **85** [7] 1725–9 (2002).

[13]J. Lu, K. Takaichi, T. Uematsu, A. Shirakawa, M. Musha, K. Ueda, H. Yagi, T. Yanagitani, and A. A. Kaminskii, "$Yb^3Y_2O_3$ Ceramics—A Novel Solid-State Laser Material," *Jpn. J. Appl. Phys.*, **41** [12A] L1373–5 (2002).

[14]Y. Huang, D. Jiang, J. Zhang, and Q. Lin, "Fabrication of Transparent Lanthanum-Doped Yttria Ceramics by Combination of Two-Step Sintering and Vacuum Sintering," *J. Am. Ceram. Soc.*, **92** [12] 2883–7 (2009).

[15]Z. A. Munir, U. Anselmi-Tamburini, and M. Ohyanagi, "The Effect of Electric Field and Pressure on the Synthesis and Consolidation of Materials: A Review of the Spark Plasma Sintering Method," *J. Mater. Sci.*, **41**, 763–77 (2006).

[16]S. Grasso, Y. Sakka, and G. Maizza, "Electric Current Activated/assisted Sintering (ECAS): A Review of Patents 1906–2008," *Sci. Technol. Adv. Mater.*, **10**, 053001, 24pp (2009).

[17]H. Yoshida, K. Morita, B.-N. Kim, K. Hiraga, M. Kodo, K. Soga, and T. Yamamoto, "Densification of Nanocrystalline Yttria by Low Temperature Spark Plasma Sintering," *J. Am. Ceram. Soc.*, **91** [5] 1707–10 (2008).

[18]R. Chaim, A. Shlayer, and C. Estournes, "Densification of Nanocrystalline Y_2O_3 Ceramic Powder by Spark Plasma Sintering," *J. Eur. Ceram. Soc.*, **29**, 91–8 (2009).

[19]B.-N. Kim, K. Hiraga, K. Morita, and H. Yoshida, "Effects of Heating Rate on Microstructure and Transparency of Spark-Plasma-Sintered Alumina," *J. Eur. Ceram. Soc.*, **29**, 323–7 (2009).

[20]K. Morita, B.-N. Kim, H. Yoshida, and K. Hiraga, "Spark-Plasma-Sintering Condition Optimization for Producing Transparent $MgAl_2O_4$ Spinel Polycrystal," *J. Am. Ceram. Soc.*, **92** [6] 1208–16 (2009).

[21]L. Smrcok, "Rietveld Refinement of Y_2O_3 using the Pearson VII Profile Shape Function," *Crystal Res. Technol.*, **24** [6] 607–11 (1989).

[22]J. E. Burke and D. Turnbull, "Recrystallization and Grain Growth"; pp. 220–92 in *Progress in Metal Physics 3*, Edited by B. Chalmers. Pergamon Press, London, 1952.

[23]M. Hillert, "On the Theory of Normal and Abnormal Grain Growth," *Acta Metal.*, **13** [3] 227–38 (1965).

[24]P.-L. Chen and I.-W. Chen, "Grain Boundary Mobility in Y_2O_3: Defect Mechanism and Dopant Effects," *J. Am. Ceram. Soc.*, **79** [7] 1801–9 (1996).

[25]Ch. Grigis and S. Schamm, "Element and Phase Identification via Fine Structure Analysis in EELS: Application to MOCVD-$Y_1Ba_2Cu_3O_{7-\delta}$ Thin Films," *Ultramicroscopy*, **74**, 159–67 (1998).

[26]A. Travlos, N. Boukos, G. Apostolopoulos, and A. Dimoulas, "Oxygen Vacancy Ordering in Epitaxial Layers of Yttrium Oxide on Si (001)," *Appl. Phys. Lett.*, **82** [23] 4053–5 (2003).

[27]F. Jollet, C. Noguera, N. Thromat, M. Gautier, and J. P. Duraud, "Electronic Structure of Yttrium Oxide," *Phys. Rev. B*, **42** [12] 7587–95 (1990).

[28]F. A. Cotton, G. Wilkinson, C. A. Murillo, and M. Bochmann, *Advanced Inorganic Chemistry*, 6th edition, pp. 1108–29. John Wiley & Sons, New York, 1999.

[29]M. P. Harmer and R. J. Brook, "Fast Firing—Microstructural Benefits," *Trans. J. Br. Ceram. Soc.*, **80** [5] 147–8 (1981).

[30]Y. Zhou, K. Hirao, Y. Yamauchi, and S. Kanzaki, "Densification and Grain Growth in Pulse Electric Current Sintering of Alumina," *J. Eur. Ceram. Soc.*, **24** [12] 3465–70 (2004).

[31]N. Murayama and W. Shin, "Effect of Rapid Heating on Densification and Grain Growth in Hot Pressed Alumina," *J. Ceram. Soc. Jpn.*, **108** [9] 799–802 (2000).

[32]G. Bernard-Granger and C. Guizard, "Densification Mechanism Involved During Spark Plasma Sintering of a Codoped Alpha-Alumina Material: Part I. Formal Sintering Analysis," *J. Mater. Res.*, **24** [1] 179–86 (2009).

[33]M. A. Clark and T. H. Alden, "Deformation Enhanced Grain Growth in a Superplastic Sn–1% Bi alloy," *Acta Metall.*, **21**, 1195–206 (1973).

[34]J. Besson and M. Abouf, "Grain Growth Enhancement in Alumina during Hot Isotatic Pressing," *Acta Metall. Mater.*, **39**, 2225–34 (1991).

[35]M. N. Rahaman, *Ceramic Processing and Sintering*, 2nd edition, pp. 482–6. Taylor & Francis, Boca Raton, 2003.

[36]D. J. Sordelet and M. Akinc, "Sintering of Monosized, Spherical Yttria Powders," *J. Am. Ceram. Soc.*, **71** [12] 1148–53 (1988).

[37]M. F. Berard, C. D. Wirkus, and D. R. Wilder, "Diffusion of Oxygen in Selected Monocrystalline Rare Earth Oxides," *J. Am. Ceram. Soc.*, **51** [11] 643–7 (1968).

[38]R. J. Gaboriaud, "Self-Diffusion of Yttrium in Monocrystalline Yttrium Oxide: Y_2O_3," *J. Solid State Chem.*, **35**, 252–61 (1980).

[39]K. Ando, Y. Oishi, H. Hase, and K. Kitazawa, "Oxygen Self-Diffusion in Single-Crystal Y_2O_3," *J. Am. Ceram. Soc.*, **66**, C222–3 (1983).

[40]M. F. Berard and D. R. Wilder, "Cation Self-Diffusion in Polycrystalline Y_2O_3 and Er_2O_3," *J. Am. Ceram. Soc.*, **52** [2] 85–8 (1969).

[41]Z.-H. Wang, P.-L. Chen, and I.-W. Chen, "Two-Step Sintering of Ceramics with Constant Grain-Size, I. Y_2O_3," *J. Am. Ceram. Soc.*, **89** [2] 431–7 (2006).

[42]M. Kodo, K. Soga, H. Yoshida, and T. Yamamoto, "Low Temperature Sintering of Polycrystalline Yttria by Transition Metal Ion Doping," *J. Ceram. Soc. Jpn.*, **117** [6] 765–8 (2009).

[43]M. Kodo, K. Soga, H. Yoshida, and T. Yamamoto, "Doping Effect of Divalent Cations on Sintering of Polycrystalline Yttria," *J. Eur. Ceram. Soc.*, **30** [13] 2741–7 (2010), in press. □

View Online / Journal Homepage / Table of Contents for this issue
Dynamic Article Links

Nanoscale

Cite this: *Nanoscale*, 2011, **3**, 3705

www.rsc.org/nanoscale

PAPER

Near-infrared (1550 nm) *in vivo* bioimaging based on rare-earth doped ceramic nanophosphors modified with PEG-*b*-poly(4-vinylbenzylphosphonate)†

Masao Kamimura,[a] Naoki Kanayama,[a] Kimikazu Tokuzen,[b] Kohei Soga[b] and Yukio Nagasaki*[acd]

Received 8th May 2011, Accepted 7th June 2011
DOI: 10.1039/c1nr10466g

A novel poly(ethylene glycol) (PEG)-based block copolymer possessing a 4-vinylbenzylphosphonate repeating unit in another segment (PEG-*block*-poly(4-vinylbenzylphosphonate)) (PEG-*b*-PVBP) was designed and successfully synthesized. As a control, an end-functionalized PEG possessing a monophosphonate group (PEG-PO_3H_2) was also synthesized. The surface of near-infrared (NIR) phosphors (*i.e.*, ytterbium (Yb) and erbium (Er) ion-codoped Y_2O_3 nanoparticles (YNPs)) were modified with PEG-*b*-PVBP (PEG-YNP(*b*)s) and PEG-PO_3H_2 (PEG-YNP(1)s). The adsorption of PEG-*b*-PVBP and PEG-PO_3H_2 was estimated by Fourier transform infrared (FT-IR) measurements and thermal gravimetric analysis (TGA). The physicochemical characteristics of the obtained YNP samples were analyzed by ζ-potential and dynamic light scattering (DLS) measurements. The ζ-potentials of YNPs modified by these polymers were close to zero, indicating the effective coverage of the YNP surface by our new PEG derivatives. However, the dispersion stability of the PEGylated YNPs was strongly affected by the structure of the PEG terminus. The average diameter of the PEG-YNP(1)s increased, and aggregates precipitated after less than 1 h in phosphate buffer saline (PBS). In contrast, the size did not change at all in the case of PEG-YNP(*b*)s and the dispersion in PBS was stable for over 1 week. PEG-YNP(*b*)s also showed high erosion resistance under acidic conditions. The multiple coordinated PVBP segment of the block copolymer on the YNP surface plays a substantial role in improving such dispersion stability. The excellent dispersion stability and strong NIR luminescence of the obtained PEG-YNP(*b*)s were also confirmed in fetal bovine serum (FBS) solution over 1 week. Furthermore, *in vivo* NIR imaging of live mice was performed, and the 1550 nm NIR emission of PEG-YNP(*b*)s from the organ of live mice was confirmed without dissection.

1. Introduction

In vivo fluorescence bioimaging has become an important technique in the biological sciences and technology because of its high sensitivity and resolution.[1–3] The technique suffers from several problems because *in vivo* fluorescence bioimaging generally employs a short wavelength excitation source, (i) the light cannot penetrate deeply due to absorption and scattering, (ii) there is high back ground interference due to significant endogenous fluorescence, and (iii) damage to biological subjects can occur. Recently, near-infrared (NIR) fluorescence bioimaging has attracted interest in this field.[4–6] Since NIR light in the wavelength region of 800 to 2000 nm the so-called "biological window",[7,8] is highly transparent *in vivo*, it penetrates deeply with less damage to the living organism. With the silicon based charge coupled device (CCD) cameras commercialized so far, the observation wavelength for fluorescence bioimaging has been limited to a maximum of 1100 nm. Recently, InGaAs CCD cameras have been developed for observation in the longer wavelength region of 800–2200 nm,[9,10] which makes not only

[a]*Department of Materials Science, Graduate School of Pure and Applied Sciences, University of Tsukuba, Tennoudai 1-1-1, Tsukuba, Ibaraki, 305-8573, Japan. E-mail: yukio@nagalabo.jp; Fax: +81-29-853-5749; Tel: +81-29-853-5749*
[b]*Department of Materials Science and Technology, Tokyo University of Science, Yamazaki 2461, Noda, Chiba, 278-8510, Japan*
[c]*Master's School of Medical Sciences, Graduate School of Comprehensive Human Sciences, University of Tsukuba, Tennoudai 1-1-1, Tsukuba, Ibaraki, 305-8573, Japan*
[d]*Satellite Laboratory, International Center for Materials Nanoarchitectonics (MANA), National Institute for Materials Science (NIMS), University of Tsukuba, Tennoudai 1-1-1, Tsukuba, Ibaraki, 305-8573, Japan*

† Electronic supplementary information (ESI) available: ^{1}H-NMR spectra of PEG-*b*-PCMS, PEG-*b*-PDEVBP and PEG-*b*-PVBP, ^{31}P-NMR spectra of PEG-*b*-PDEVBP and PEG-*b*-PVBP, schematic representation of PEG-PO_3H_2 synthesis, ^{1}H-NMR spectra of PEG-PO_3Et_2 and PEG-PO_3H_2, FT-IR spectra of YNP samples, PEG brush density on the YNP surface, and size distribution of YNP samples under acidic conditions are described. See DOI: 10.1039/c1nr10466g

excitation but also illumination feasible for new NIR bioimaging techniques. On the basis of these developments, bioimaging is now shifting gradually from short wavelength to NIR.

Rare-earth ion-doped ceramic nanophosphors (RED-CNPs) are known to fluoresce efficiently in the NIR wavelength region under NIR excitation. For example, a 1550 nm emission under 980 nm excitation from Er^{3+} doped in silicate glass fibers is used for optical communications.[10] One of the specific fluorescence modes of the RED-CNPs is visible light emission under NIR excitation, which is termed as an upconversion emission due to stepwise absorption among the discrete energy levels of the RED-CNPs.[11–14] We have already reported the application of the upconversion emission of ytterbium (Yb) and erbium (Er) ion-codoped yttrium oxide (Y_2O_3) nanoparticles (YNPs) as a bioimaging probe.[15] The YNPs are known to show upconversion emissions at 550 nm and 660 nm when excited at 980 nm.[13–15] The YNPs also shows a 1550 nm emission when excited at 980 nm.[9] Recently, the number of reports of upconversion emissions of RED-CNPs in bioimaging has been increasing,[16–20] and investigations of the applicability of various RED-CNPs as *in vivo* fluorescence bioimaging agents have been carried out.[21–25] In most of the earlier studies, however, visible emissions were observed by upconversion. As far as we know, no 1550 nm NIR emission of RED-CNPs has been reported as *in vivo* bioimaging probe. In this report, we establish *in vivo* bioimaging by both NIR excitation and emission using new RED-CNPs.

The effective implementation of *in vivo* bioimaging requires the improvement of the blood circulation of RED-CNPs. To this end, the construction of a poly(ethylene glycol) (PEG) brush layer on the surface of nanoparticles is widely carried out for improvement of the dispersion stability and blood circulation of nanoparticles. PEG is a well known biocompatible polymer,[26–28] and PEG grafted to the surfaces of nanoparticles also serves to their biocompatibility. Surface-tethered PEG chains aid the dispersion of the nanoparticles in water by the steric repulsion. Our group has reported the preparation of several kinds of PEG modified nanoparticles.[27,28] Recently, we have also reported the surface modification of YNPs with PEG-*b*-poly(acrylic acid) (PAAc) as an upconversion bioimaging probe.[15] Although the PEG-*b*-PAAc modified YNPs showed high dispersion stability in Tris–HCl buffer (10 mM, pH 7.4, 150 mM NaCl) and sufficiently good performance for *in vitro* biolabeling, the PEG brush density of PEG-*b*-PAAc on the surface of YNPs was not high enough compared to that of other PEGylated nanoparticles such as gold nanoparticles.[29,30] The very low coordination ability of the side chain carboxylic acid groups of the PAAc segment in the block copolymer might be one of the reasons for the low PEG chain density. To further improve the performance of YNPs *in vivo* environment, a suitable design for a PEG based polymer for modification of the YNP surface is required.

Since the phosphonate group is well known to bind to the surface of YNPs[31,32] and other metal oxides,[33–35] it would be a suitable candidate for improving the binding stability of the PEG brush on the surface of the YNP. Prior research on terminal-phosphate PEG for nanoparticle modification has been reported.[32,36–38] Since blood is a very complex medium, however, substantial effort is required to improve the surface characteristics of YNPs for *in vivo* applications. We have examined the multi-point anchoring of PEG on a substrate surface using a block copolymer possessing an anchoring moiety as a side chain in one of the segments.[27] For example, PEG-*b*-poly((2-*N*,*N*-dimethylamino)ethyl methacrylate) (PEG-*b*-PAMA) coordinated efficiently to a gold nanoparticle surface, effecting excellent stabilization.[29] The multi-point coordination of the lone pair of the amino group in the PAMA segment played a substantial role. Polyvalent coordination by one of the block copolymer segments is believed to be a rational design for the application of nanoparticles *in vivo*.

In order to confirm the effect of multi-point coordination on the YNP surface, a new block copolymer, PEG-*b*-poly(4-vinylbenzylphosphonate) (PEG-*b*-PVBP) was designed (Scheme. 1). Our idea was to increase the stability of the block copolymer on the YNP surface through multi-point coordination of phosphonate groups in the PVBP segment in addition to the hydrophobic nature of the polystyrene segment, which tends to be excluded from aqueous media and directed to the nanoparticle surface. As a control, PEG possessing a mono-phosphonate end group (PEG-PO_3H_2) was also synthesized to compare the block copolymer modification.

This report deals with the synthesis of the new block copolymer and its use in the subsequent surface modification of YNPs for utilization as *in vivo* bioimaging probes. The *in vivo* NIR fluorescence bioimaging of live mice was also examined. This is the first demonstration of *in vivo* NIR fluorescence bioimaging of live mice using the 1550 nm NIR emission of RED-CNPs.

2. Materials and methods

2.1 Materials

α-Methoxy-ω-mercapto-poly(ethylene glycol) (PEG-SH, M_n = 5000 g mol^{-1}) was purchased from NOF Corporation (Tokyo, Japan) and used without further purification.

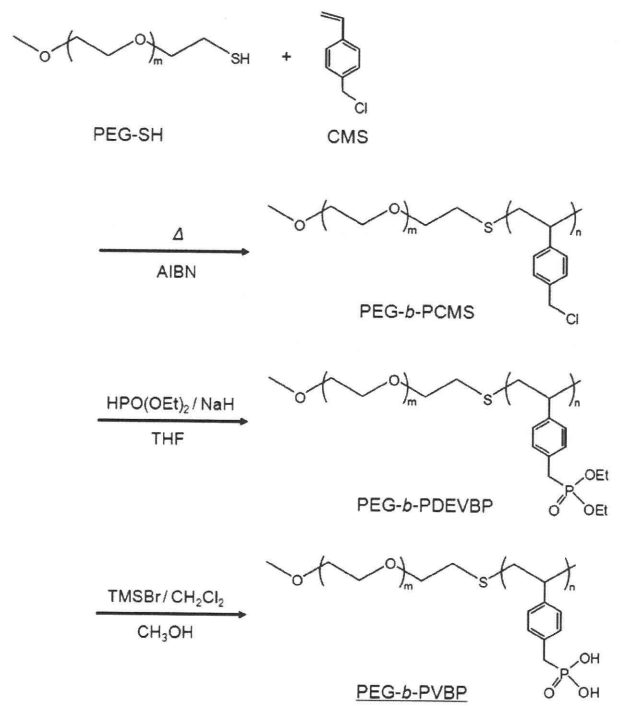

Scheme 1 Schematic representation of PEG-*b*-PVBP synthesis.

4-Chloromethylstyrene (CMS) was kindly provided by Seimi Chemical Co. Ltd., (Kanagawa, Japan) and purified on a silica gel column to remove the inhibitor, followed by vacuum distillation under a nitrogen atmosphere. 2,2′-Azobisisobutyronitrile (AIBN; Kanto Chemicals Co. Ltd., Tokyo, Japan) was purified by recrystallization from methanol. Tetrahydrofuran (THF; Kanto Chemicals) was passed through purification columns (Glass Contour Solvent Dispensing System, HANSEN & Co., Ltd.) before use. 2-Methoxyethanol (Wako Pure Chemical Industries, Ltd., Osaka, Japan) and ethylene oxide (EO; 100%; Sumitomo Seika Chemicals Co., Ltd, Hyogo, Japan) were purified conventionally.[39] A THF solution of potassium naphthalene (K-naph) was prepared by a method described previously.[40] Dichloromethane (CH_2Cl_2; Kanto Chemicals) was dried over calcium hydride and distilled. Diethyl phosphite, diethyl 2-bromoethylphosphonate, trimethylsilyl bromide (TMSBr; Tokyo Chemical Industry, Co., Ltd, Japan), sodium hydride (NaH; 55% oil dispersion, Kanto Chemicals), sodium iodide (NaI), yttrium nitrate hexahydrate, erbium nitrate pentahydrate, ytterbium nitrate hydrate, urea, fetal bovine serum (FBS) (Wako Pure Chemical Industries), 2-propanol, diethylether, methanol, and benzene (Kanto Chemicals) were used without further purification.

2.2 Synthesis of PEG-*b*-PVBP

PEG-*b*-poly(4-chloromethylstyrene) (PEG-*b*-PCMS) was synthesized by the radical telomerization of CMS using PEG-SH as a telogen, according to the procedure described in our previous report.[41] Briefly, PEG-SH (1.0 g, 0.2 mmol), CMS (1.53 g, 10.0 mmol) and AIBN (16.5 mg, 0.1 mmol) were weighed into flask and dissolved in 20 mL of toluene. The solution was degassed through three freeze–thaw–evacuate cycles. Polymerization was conducted for 24 h at 60 °C under the nitrogen atmosphere. The resulting polymer was then purified by repeating precipitation into *n*-hexane and diethylether. The recovered polymer was finally freeze-dried with benzene to obtain PEG-*b*-PCMS (1.25 g, yield 85%). The polymerization degree of PCMS segment (*n*) was determinated as $n = 16$ by ^{1}H-NMR analysis, assuming the number-averaged molecular weight (M_n) of the PEG segment to be 5000 g mol^{-1} (ESI, Fig. S1(1)†). The side chains of the PCMS segment were converted to diethylphosphonate (PEG-*b*-poly(diethyl-4-vinylbenzylphosphonate) (PEG-*b*-PDEVBP)) by the Michaelis–Becker reaction.[42] NaH (126 mg, 5.25 mmol) and NaI (*ca.* 40 mg) were weighted into a flask and dispersed in 5 mL of THF. After cooling to 0 °C with magnetic stirring, diethyl phosphite (0.33 mL, 2.55 mmol) was slowly added over 5 min, and the reaction mixture was further stirred for 20 min. A solution of PEG-*b*-PCMS (500 mg) in 5 mL of THF was added drop wise to the mixture at 0 °C, and then, the mixture was warmed gradually to room temperature and stirred for 12 h. After stirring, the solvent was removed by evaporation. The obtained polymer was purified by dialysis (Spectra/Por 6, MWCO 3,500, SPECTRUM) for 2 days against excess methanol (2 L), which was changed after 2, 4, 8, 18, and 32 h. The final solution was concentrated under reduced pressure, followed by freeze-drying with benzene (490 mg, yield: 94%) (ESI, Fig. S1 (2)†). The diethylphosphonate moiety of the obtained PEG-*b*-PDEVBP was hydrolyzed to the corresponding by treatment with TMSBr followed by methanolic hydrolysis.[43,44] Briefly, PEG-*b*-PDEVBP (430 mg) was weighted into a flask, TMSBr (0.47 mL, 3.55 mmol) in 5 mL of dichloromethane was added and the solution was refluxed for 2 h at 45 °C. After evaporation of the solvent, 20 mL of methanol was added, and the mixture was stirred at room temperature for 15 h. After stirring, the solvent was removed by evaporation. The obtained polymer was purified by dialysis (Spectra/Por 6, MWCO 3,500, SPECTRUM) for 2 days against excess methanol (2 L), which was changed after 2, 4, 8, 18, and 30 h. The final product was concentrated under reduced pressure, followed by freeze-drying with benzene to obtain PEG-*b*-PVBP (378 mg, yield: 91%) (ESI, Fig. S2†).

2.3 Synthesis of PEG-PO_3H_2

A PEG possessing a methoxy group at the α-chain and a hydroxyl group at the ω-end (PEG-OH) ($M_n = 5200$, $M_w/M_n = 1.01$) was synthesized by ring-opening anionic polymerization according to a previously described method.[29] The ω-end of PEG-OH was converted to diethylphosphonate group (PEG-PO_3Et_2). Briefly, PEG-OH (2.0 g, 0.38 mmol), NaH (0.096 g, 4 mmol) and NaI (*ca.* 40 mg) were loaded into a round bottom flask equipped with a three-way stop cock, followed by three vacuum and nitrogen purging cycles. THF (10 mL) was added to the flask, and the mixture was stirred for 20 min at room temperature. After stirring, diethyl 2-bromoethylphosphonate (0.49 g, 2 mmol) was added and the reaction mixture was stirred for 36 h at room temperature. Excess NaH in the reaction mixture was removed by filtration, and the polymer was precipitated from 2-propanol. The precipitate was collected by centrifugation (5000 rpm, 15 min, 4 °C, 3 times). The recovered polymer was finally freeze dried with benzene to obtain PEG-PO_3Et_2 (1.75 g, yield: 85%). The diethylphosphonate moiety of the obtained PEG-PO_3Et_2 was hydrolyzed to give the corresponding phosphonate by treatment with TMSBr followed by methanolic hydrolysis as follows.[43,44] PEG-PO_3Et_2 (1.5 g) was weighted into a flask, TMSBr (0.22 g, 1.45 mmol) in 50 mL of dichloromethane was added, and the solution was refluxed for 2 h at 45 °C. After evaporation of the solvent, 50 mL of methanol was added, and the mixture was stirred at room temperature for 15 h to methanolic hydrolysis. The resultant product was purified by pouring the solution into 2-propanol to precipitate the polymer, which was collected by centrifugation (5000 rpm, 15 min, 4 °C, 3 times). The recovered polymer was finally freeze-dried with benzene to obtain PEG-PO_3H_2 (1.29 g, yield 87%).

2.4 Praparation of PEGylated YNPs

Ytterbium and erbium ion-codoped Y_2O_3 (Y_2O_3 : Yb, Er) nanoparticles (YNPs) were prepared by the homogeneous precipitation method, according to a previously reported procedure.[15,45] PEG-*b*-PVBP modified YNPs (PEG-YNP(*b*)s) were prepared as follows. Ten mg of YNPs was dispersed in 1.0 mL of THF and sonicated for 1 h at room temperature. PEG-*b*-PVBP (50.0 mg) was added to the YNP dispersion. The mixture was stirred for 24 h at room temperature, after which, THF was removed by evaporation and the samples were vacuum dried for 12 h at 50 °C. The excess free polymer was removed by ultracentrifugation (1.0×10^4 *g*, 15 min, 3 times), and the solvent

was changed to phosphate buffer saline (PBS) (10 mM, pH 7.4, 150 mM NaCl). PEG-PO_3H_2 modified YNPs (PEG-YNP(1)s) were also prepared by the same method (10.0 mg and 50.0 mg of YNPs and PEG-PO_3H_2, respectively). The final concentrations of both PEG-YNP(*b*)s and PEG-YNP(1)s were 1.0 g L^{-1}.

2.5 Evaluation of PEGylated YNPs characteristics

The surface charge of the PEG-YNP(1)s and PEG-YNP(*b*)s were measured by means of a ζ-potential analyzer (ZetasizerNano ZS, Malvern Instruments, Ltd., U.K.) in 10 mM NaCl solution. The adsorption of the polymer was confirmed by the Fourier transform infrared (FT-IR) spectrum, which was recorded by an FT/IR-6200 (JASCO, Japan). The samples for FT-IR were prepared by the following method. The solvent of the YNP samples dispersion was changed to pure water by ultracentrifugation (1.0×10^4 *g*, 15 min, 3 times) and the YNP samples dispersion was freeze-dried for 24 h. The obtained YNP samples were milled with KBr and pressed into a pellet for analysis (1 wt% in KBr). The PEG density on the YNP surface was evaluated by thermal gravimetric analysis (TGA) (SHIMADZU DTG-60). Images of YNP samples were obtained *via* scanning electron microscopy (SEM) (HITACHI S-4200). The SEM samples were prepared by placing a drop of the YNPs dispersion (0.1 g L^{-1}) on a silicon wafer and drying at 110 °C for 5 min. The size distribution of the YNP samples in PBS (10 mM, pH 7.4, 150 mM NaCl) was evaluated by dynamic light scattering (DLS) (ZetasizerNano ZS) equipped with a He–Ne laser that produces vertically polarized incident beams at a detection angle of 173° at room temperature. The surface charge of the YNP samples after dispersion in PBS was measured by ζ-potential analyzer (ZetasizerNano ZS). The PBS solvent of the YNP sample solution was displaced to 10 mM NaCl solution (pH 7.4) by ultracentrifugation (1.0×10^4 *g*, 15 min, 3 times), followed by ζ-potential measurements was performed.

2.6 Characterization of the stability of YNP samples under acidic conditions

The acid erosion resistance of YNP samples under acidic conditions (pH 5.0) was evaluated by measurement of the time dependent variation of the pH. The size distribution of the YNP samples under acidic conditions (pH 5.0) was also evaluated by DLS (ZetasizerNano ZS). The initial concentrations of the sample solutions were 1.0 g L^{-1}.

2.7 Characterization of YNP samples in fetal bovine serum solution

To confirm the dispersion stability of the YNP samples in serum solution, after the obtained YNP samples were precipitated by ultracentrifugation (1.0×10^4 *g*, 15 min, 3 times) and the solvent was substituted with FBS solution (10 mM PB, pH 7.4, 150 mM NaCl, 10% FBS). The final concentrations of the solutions were 0.1 g L^{-1}. The size distribution of the YNP samples in FBS solution was evaluated by DLS (ZetasizerNano ZS). The NIR emission spectra of the YNP samples in FBS solution were obtained using a spectrometer (Avaspec-NIR256–1.7, Avantes, Netherlands) equipped with a NIR excitation source (LU0975T050, Lumics, Germany) and laser diode (SLI-CW-9MM-C1-980-1M-PD, Semiconductor Laser International Corp., USA). The NIR luminescence of the YNP samples in FBS solution was confirmed by observation with an InGaAs CCD camera (NIR-300PGE, VDS Vosskühler, Germany) equipped with a NIR excitation source (LU0975T050) and laser diode (SLI-CW-9MM-C1-980-1M-PD).

2.8 *In vivo* near-infrared fluorescence imaging of live mice

The *in vivo* NIR fluorescence imaging study was carried out using the NIR bioimaging system, consisting of a 980 nm fiber pigtailed diode laser (LD, SLI-CW-9MM-C1-980-1M-PD), NIR excitation source (LU0975T050), a laser scanner (VM500+, GSI Group, USA) for planar irradiation of the excitation light, and InGaAs CCD camera (NIR-300PGE) for detection of the NIR fluorescence. Male ICR mice (8 weeks old, *ca.* 25 g) were purchased from Charles River Japan, Inc. Each YNP group contained three mice. The YNPs dispersion in physiological saline was intravenously administrated to mice at a dose of 10 mg. The mice were kept in a cage for 24 h and subjected live to NIR fluorescence imaging after anesthetization. After the live imaging experiments, the mice were sacrificed to obtain several organs for direct imaging. All procedures and animal care were approved by the Committee on the Ethics of Animal Experimentation of the University of Tsukuba, and were conducted according to the Guidelines for Animal Experimentation of the University of Tsukuba.

3. Results and discussion

3.1 Synthesis of PEG-*b*-PVBP and PEG-PO_3H_2

PEG-*b*-PVBP was synthesized by the side chain conversion of PEG-*b*-PCMS, as shown in Scheme 1. Complete side chain conversion of PEG-*b*-PCMS was confirmed by ^{1}H-NMR analysis (ESI, Fig. S1†). The diethylphosphonate moiety was hydrolyzed to give the phosphonate group by treatment with TMSBr followed by methanolic hydrolysis. Complete hydrolysis was suggested by both the disappearance of proton signals assigned to the diethylester moiety (ESI, Fig. S2†) and the change in the chemical shift of ^{31}P-NMR (ESI, Fig. S3†). As a control, PEG-PO_3H_2 was synthesized according to the procedure as shown in Scheme S1 in the ESI†. Complete conversion of the ω-end of PEG-OH was confirmed by ^{1}H-NMR analysis (ESI, Fig. S4†). From the SEC measurement, the M_n and M_w/M_n of PEG-PO_3H_2 were determined to be 5200 g mol^{-1} and 1.01, respectively, based on PEG calibration.

3.2 Preparation and characterization of PEGylated YNPs

YNPs were synthesized by the homogeneous precipitation method.[15,45] The charge on the YNP surface was about +20 mV in 10 mM NaCl solution (pH 7.4), which was in good agreement with our previous report.[15] The average grain diameter of the YNPs was about 100–200 nm, as confirmed by SEM measurement (Fig. 1(a)). These results suggest that YNPs were successfully synthesized.

PEGylation of the YNP surface was then carried out using the prepared polymers as mentioned above. To confirm the adsorption of polymer on the YNP surface, the surface charge on

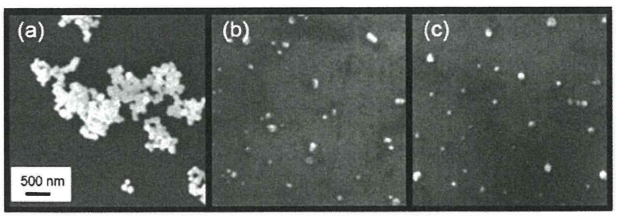

Fig. 1 SEM images of YNP samples. (a) native-YNPs, (b) PEG-YNP(1)s, and (c) PEG-YNP(*b*)s. (SEM measurement: accelerating voltage 5.0 kV).

the YNPs was estimated. Fig. 2 shows the change in the ζ-potential of native-YNPs and polymer modified YNPs with pH ranging from 5 to 13. After PEGylation of the YNPs, the free polymer in the solution was removed by repeated ultracentrifugation, and the solvent was changed to 10 mM NaCl solution with various pH values. The ζ-potential of the native-YNPs was about +20 mV at pH 7.4, as mentioned above, and it increased with decreasing pH. In contrast, the ζ-potential of the polymer modified YNPs were close to zero regardless of the environmental pH. Notably, the ζ-potential of PEG-YNP(*b*)s was much closer to zero than that of PEG-YNP(1)s though PEG-*b*-PVBP possesses a much higher negative charge than does PEG-PO_3H_2. These results suggest that the phosphonate segment in the block copolymer was adsorbed on the YNP surface, allowing the PEG segment to be tethered from the surface into the aqueous environment to shield the surface charge.

Polymer adsorption on the YNP surface was also confirmed by FT-IR measurements. All samples were prepared by freeze drying after the solution was purified by repeated ultracentrifugation and the solvent was changed to water. Fig. S5 in the ESI† shows the FT-IR spectra of the PEG-YNP(1)s (a) and PEG-YNP(*b*)s (b) samples. Native-YNPs did not exhibit the adsorption bands at 960, 1100, 1240, 1460, and 2890 cm^{-1} that are attributable to the P–OH stretches, C–O–C stretches, P=O stretches, P–C stretches, and C–H stretches in PEG-PO_3H_2 and PEG-*b*-PVBP, respectively. After the surface modification of the

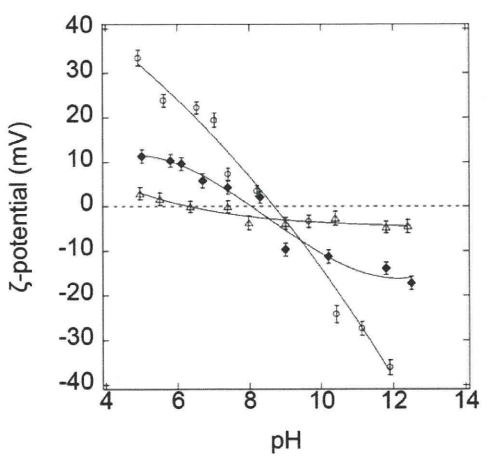

Fig. 2 Change in the ζ-potential of YNP samples with pH ranging from 5 to 13. (Open circles) Native-YNPs, (close diamonds) PEG-YNP(1)s, and (open triangles) PEG-YNP(*b*)s (ζ-potential measurement: room temperature; 10 mM NaCl solution).

YNPs with PEG-PO_3H_2 and PEG-*b*-PVBP, adsorption peaks derived from the polymers were clearly observed despite repeated ultracentrifugation treatments.

In order to quantitatively confirm the extent of adsorption of the polymer on the surface of the YNPs, TGA measurements of the YNP samples were carried out. Table S1 in the ESI† shows the TGA results for the PEGylated YNPs. The weight losses of PEG-YNP(1)s and PEG-YNP(*b*)s at 900 °C were 11.0 and 2.1%, respectively. From the data, the PEG chain densities of the PEG-PO_3H_2 and PEG-*b*-PVBP on the YNP surface were estimated to be 1.30 and 0.14 chains nm^{-2}, respectively. These densities were higher than those of the PEG-*b*-PAAc modified YNPs (0.019 chains nm^{-2}), as described previously.[15] These results show that the phosphonate groups of PEG-PO_3H_2 and PEG-*b*-PVBP are strongly bound to the YNP surface compared with the carbonyl group of PEG-*b*-PAAc. In addition, because PEG-*b*-PVBP possesses a long anchor segment, the value of the PEG brush density for PEG-*b*-PVBP was lower than that for PEG-PO_3H_2. Therefore, considering the PEG brush density, PEG-PO_3H_2 was a good surface modification agent.

The dispersion stability of YNP samples was visually assessed by SEM imaging. Fig. 1 shows the SEM images of (a) native-YNPs, (b) PEG-YNP(1)s and (c) PEG-YNP(*b*)s. In the case of native-YNPs, large agglomerates were observed, while PEGylated YNPs were well-dispersed with almost no agglomeration. The particle size of the PEGylated YNPs was about 100–200 nm. We further evaluated the long term dispersion stability of YNP samples in PBS by DLS measurement. The variations in the size distribution of native-YNPs, PEG-YNP(1)s and PEG-YNP(*b*)s are shown in Fig. 3(a)–(c), respectively. The YNP samples were dispersed in PBS, the average particle sizes of these YNPs were about 200 nm just after dispersion. However, the native-YNPs immediately agglomerated and precipitated in less than 30 min. Although the dispersion stability of the YNPs was slightly increased by surface modification with PEG-PO_3H_2, the average diameter of the PEG-YNP(1)s also increases significantly in less than 1 h. In contrast, the average diameter and its distribution of the PEG-YNP(*b*)s did not increase, and the dispersion remained stable in PBS over a period of 1 week. This result indicates that the modification by PEG-*b*-PVBP affords much higher dispersion stability than that by PEG-PO_3H_2, though the surface PEG density of PEG-YNP(*b*)s was lower than that of PEG-YNP(1)s. On the basis of these findings, it was concluded that PEG-*b*-PVBP was firmly adsorbed and formed an ideal PEG brush layer on the YNP surface. In order to further evaluate the stabilities of the YNP samples in PBS, ζ-potentials were measured after dispersion in PBS. Fig. 4 shows the ζ-potential measurement results for (a) native-YNPs, (b) PEG-YNP(1)s, and (c) PEG-YNP(*b*)s, respectively. As shown in Fig. 4(a), the ζ-potential of the native-YNPs was about +20 mV in 10 mM NaCl solution (pH 7.4), while it converted to a negative charge (−19 mV) after dispersion in PBS, indicating the adsorption of the phosphate salt on the YNP surface. Goff *et al.* reported that a phosphate salt of PBS was adsorbed on the surface of Fe_3O_4 NPs.[38] Our result was in good agreement with this report. The ζ-potential of the PEG-YNP(1)s also decreased from +4.3 mV to −13.7 mV after dispersion in PBS, suggesting that PEG chain liberated from the particle surface by the exchange with phosphate salt in media. In contrast, the ζ-potential of the PEG-YNP(*b*)s was

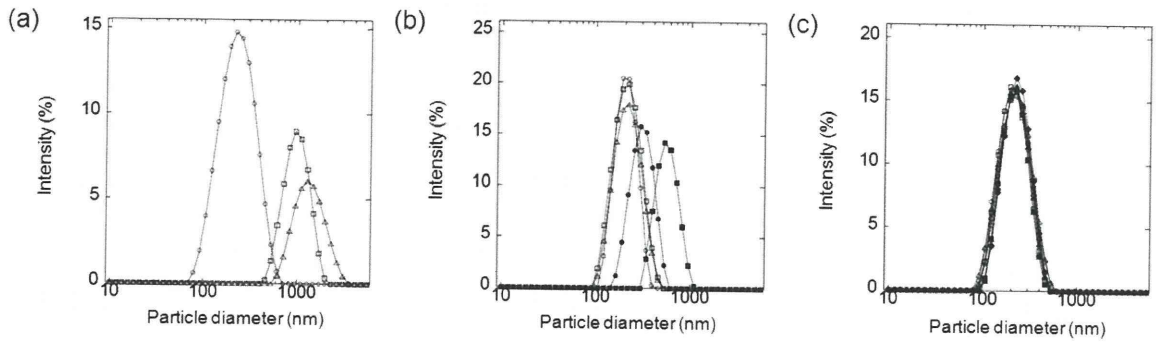

Fig. 3 Variation with time of the size distribution of YNP samples in PBS (10 mM PB, pH 7.4, 150 mM NaCl). (a) Native-YNPs. (Open circles) 0 min, (open squares) 10 min, and (open triangles) 20 min. (b) PEG-YNP(1)s. (Open circles) 0 min, (open squares) 10 min, (open triangles) 20 min, (close circles) 50 min, and (close squares) 70 min. (c) PEG-YNP(*b*)s. (Open circles) 0 day, (open squares) 1 day, (open triangles) 2 days, (open diamonds) 3 days, (close circles) 4 days, (close squares) 5 days, (close triangles) 6 days, and (close diamonds) 7 days. (DLS measurement: room temperature).

close to zero and it did not change after dispersion in PBS. Multivalent coordination of the PVBP segment in the block copolymer might hinder exchange with phosphate ion in media.

3.3 Characterization of the stability of YNP samples under acidic conditions

It is well known that the native-YNPs erode under acidic conditions (pH < 6.8). When the YNPs are thus eroded, the pH value of the YNPs solution increases according to eqn (1).

$$Y_2O_3 + 6H^+ \rightarrow 2\ Y(OH)_3 \quad (1)$$

We reported recently that the erosion of YNP was retarded by surface modification, which was monitored by the change in the pH value of medium.[46] As is evident in Fig. 5, the pH of the solution increased rapidly and attained a constant value (pH 7.0) after only 20 min when native-YNPs were exposed to acidic media (pH 5.0). When PEG-YNP(1)s were exposed to the same conditions, the rate of pH variation decreased, indicating retardation of erosion. In fact, 80 min were required for the complete erosion of PEG-YNP(1)s. It is interesting to note that no pH variation was observed during the acid treatment of PEG-YNP(*b*)s. Complete coverage of the YNP by PEG-*b*-PVBP might play a substantial role in preventing the erosion of the YNPs.

In addition to the pH variation tests, the long term dispersion stabilities of the YNP samples under acidic conditions were also investigated by DLS measurements. The variation of the sizes and their distribution of native-YNPs, PEG-YNP(1)s and PEG-YNP(*b*)s are shown in Fig. S6(a)–(c) in the ESI† respectively. The YNP samples were dispersed in acidic solution (pH 5.0), the average particle sizes of these YNPs were about 200 nm just after preparation of the sample solutions. Because the native-YNPs easily dissolve at pH 5.0, the average particle size of native-YNPs immediately decreased in less than 30 min. Although the rate of erosion of PEG-YNP(1)s was delayed to some extent, the size of the particle gradually decreased. Finally, size analysis confirmed that the average particle sizes of PEG-YNP(*b*)s did not change at all, and the dispersion remained stable at least over a period of 2 days. These results agreed well with the pH valuation in acidic media as shown in Fig. 5. From these data, we concluded that the

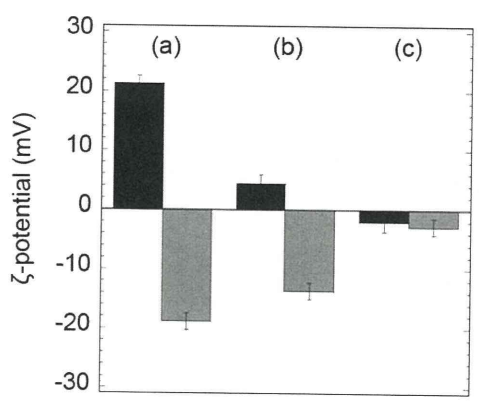

Fig. 4 ζ-Potential of YNP samples in water (black bar) and after dispersion in PBS (10 mM PB, pH 7.4, 150 mM NaCl) (gray bar). (a) Native-YNPs, (b) PEG-YNP(1)s, and (c) PEG-YNP(*b*)s. The water and PBS solvent were displaced to 10 mM NaCl solution (pH 7.4), respectively, ζ-potential measurement was performed (ζ-potential measurement: room temperature).

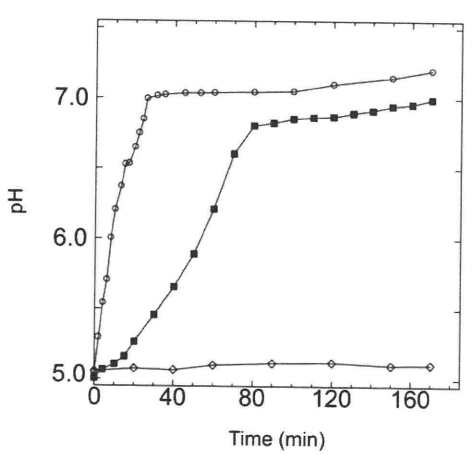

Fig. 5 pH changes of the YNP samples under acidic conditions. (Open circles) native-YNPs, (close squares) PEG-YNP(1)s, and (open diamonds) PEG-YNP(*b*)s (pH measurement: room temperature).

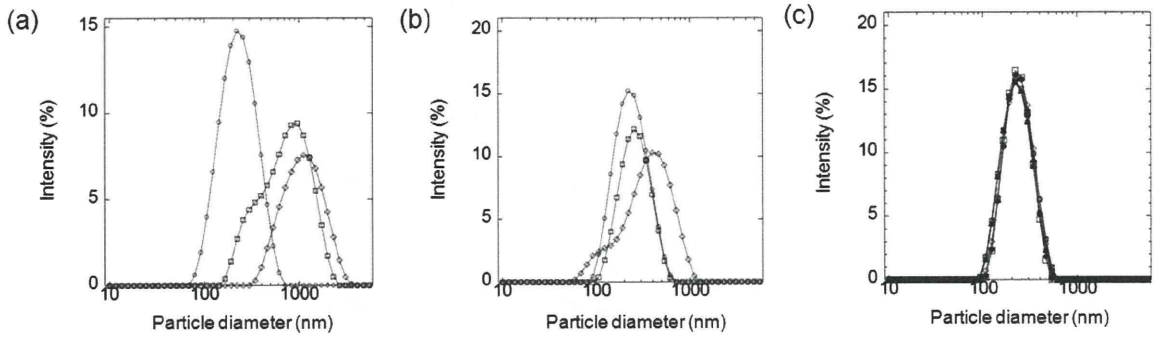

Fig. 6 Variation with time of the size distribution of YNP samples in FBS solution (10 mM PB, pH 7.4, 150 mM NaCl, 10% FBS). (a) Native-YNPs. (Open circles) 0 min, (open squares) 5 min, and (open diamonds) 10 min. (b) PEG-YNP(1)s. (Open circles) 0 min, (open squares) 10 min, and (open diamonds) 20 min. (c) PEG-YNP(*b*)s. (Open circles) 0 day, (open squares) 1 day, (open triangles) 2 days, (open diamonds) 3 days, (close circles) 4 days, (close squares) 5 days, (close triangles) 6 days, and (close diamonds) 7 days (DLS measurement: room temperature).

surface of the YNPs was completely covered with PEG-*b*-PVBP. The hydrophobic layer formed by the polystyrene segment might be supported to improve such marked high resistance against acid erosion.

3.4 Characterization of YNPs in fetal bovine serum solution

Characterization of the dispersion stability in serum is one of the most important requirements for *in vivo* imaging because it ensures stable administration *via* intravenous injection. The

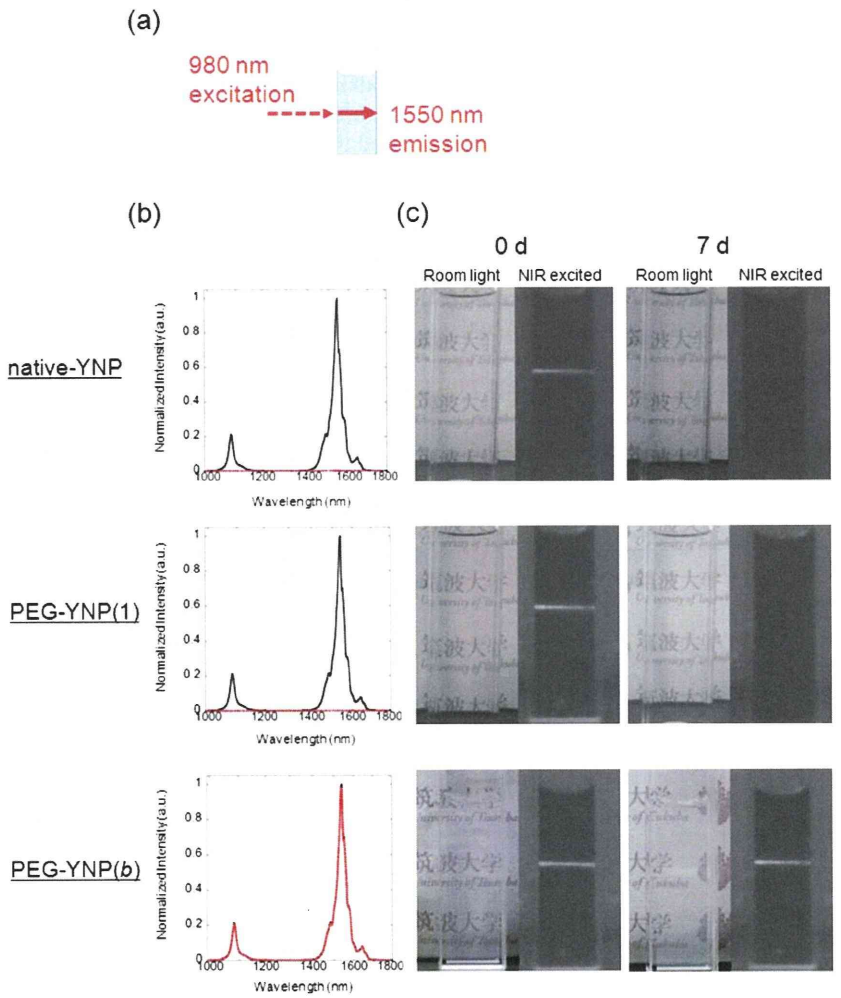

Fig. 7 Near-infrared luminescence observation of YNP samples in FBS solution (10 mM PB, pH 7.4, 150 mM NaCl, 10% FBS). (a) Schematic representation of luminescent observation. (b) Emission spectra of YNPs in FBS solution. (Black) 0 day and (Red) 7 days. (c) Luminescent observation images of YNPs in FBS solution. (Emission measurement: room temperature; excitation wavelength, 980 nm; laser strength, 650 mW cm^{-2}.)

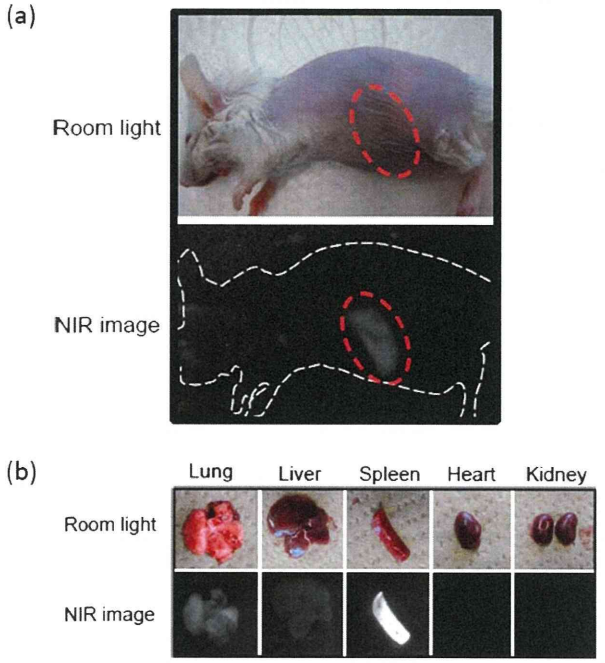

Fig. 8 *In vivo* near-infrared imaging of living mouse with intravenous injection of PEG-YNP(*b*)s. (a) Whole body and (b) various organs. (Emission measurement: room temperature; excitation wavelength, 980 nm; laser strength, 700 mW cm^{-2}).

long term dispersion stability of YNP samples in FBS solution was evaluated by DLS measurement. The variation of the size distribution of native-YNPs, PEG-YNP(1)s and PEG-YNP(*b*)s are shown in Fig. 6(a)–(c), respectively. The average particle sizes of these YNPs were about 200 nm just after preparation of the sample solution. As in the case of PBS solution, although the dispersion stability of YNP was slightly improved by the surface modification with PEG-PO_3H_2, the average diameter of native-YNPs and PEG-YNP(1)s were easily increased in less than 30 min. These results indicate that both the native-YNPs and PEG-YNP(1)s might interact with serum proteins to agglomerate and rapidly clog blood vessels. Such agglomeration tendencies cause severe problems when these YNPs are administered systematically *via* intravenous injection. The average diameter and its distribution of the PEG-YNP(*b*)s did not change at all, and the dispersion remained stable in FBS solution over a period of 1 week. Very few non-specific interactions of PEG-YNP(*b*)s with serum proteins might occur to improve its dispersion stability.

The NIR luminescence of YNP samples was then evaluated in FBS solution. As shown in Fig. 7, these YNP samples show strong 1550 nm emission (EX. 980 nm) in FBS solution just after preparation (0 day). After 1 week, however, almost no emission was observed for native-YNPs and PEG-YNP(1)s, which is explained by the precipitation of these YNPs in FBS as stated above. In contrast, the PEG-YNP(*b*)s showed high dispersion stability and emitted strong NIR luminescence in FBS solution after 1 week. Thus, real dispersion stable YNPs with high NIR luminescence in serum solution were obtained by using our newly designed block copolymer, PEG-*b*-PVBP.

3.5 *In vivo* near-infrared fluorescence imaging of live mice

As a demonstration of the use of YNPs as an *in vivo* NIR bioimaging probe, YNP samples were injected into mice. The live mice and organs were observed by an NIR bioimaging system. However, all mice perished just after intravenous injection in the case of native-YNPs and PEG-YNP(1)s. The agglomeration character as well as surface erosion might influence this acute toxicity. In contrast, all mice survived after intravenous injection of PEG-YNP(*b*)s under these experimental conditions. These results indicate that the complete surface coverage of YNP with PEG-*b*-PVBP dramatically improves the blood circulation of YNPs. Whole body images of a live mouse 24 h after injection of PEG-YNP(*b*)s are shown in Fig. 8(a). The hair of mice was removed before NIR imaging experiments. From this result, the emission of PEG-YNP(*b*)s from the spleen was confirmed without dissection. In addition, Fig. 8(b) shows *ex vivo* NIR images of dissected organs from the same mouse sacrificed after live imaging 24 h after injection of PEG-YNP(*b*)s. These results show high levels of emission in the lung, liver, and spleen, indicating a high uptake of PEG-YNP(*b*)s by these organs. In this study, we used relatively large size YNPs (d = 200 nm) and therefore these YNPs accumulated in the liver and spleen. Further *in vivo* imaging experiment using our PEG-YNP(*b*)s are now in progress and detailed investigation will be published elsewhere.

4. Conclusions

A newly designed PEG block copolymer, PEG-*b*-PVBP was successfully synthesized. As a control, an end-functionalized PEG, PEG-PO_3H_2 was also synthesized. The surfaces of YNPs were modified with PEG-*b*-PVBP and PEG-PO_3H_2. The surface charge of the YNPs was effectively shielded by the PEG brush over a wide pH range (5–13). When mono-functional PEG-PO_3H_2 was used as a surface modification agent, densely packed PEG chains were tethered on the YNP surface (PEG-YNP(1)s). When the PEG-YNP(1)s were exposed to PBS or serum protein solution, however, facile agglomeration occurred due to replacement and/or non-specific adsorption. Administration of PEG-YNP(1)s to mice *via* tail vein injection causes acute death. In contrast, our newly designed block copolymer, PEG-*b*-PVBP could be adsorbed on a YNP surface to form an extremely stable complex, PEG-YNP(*b*)s which did not agglomerate in any of PBS, acid, or serum protein solutions. Furthermore, all mice survived intravenous injection of PEG-YNP(*b*)s *via* tail vein. The 1550 nm emission of PEG-YNP(*b*)s from the organs of live mice was confirmed without dissection. This is the first reported instance of *in vivo* NIR imaging of small living animals without dissection, the imaging is based on 1550 nm emission of RED-CNPs. Therefore, PEG-YNP(*b*)s are a promising candidate for use in the development of novel *in vivo* NIR imaging probes.

Acknowledgements

We are grateful to Mr Masato Tamura for assistance with animal studies. This research was partially supported by a Grant-in-Aid for Scientific Research on Innovative Areas (Soft Interface), no. 20106011, from the Ministry of Education, Science, Sports and Culture of Japan. M. K. is also grateful for the research fellowship of the Japan Society for the Promotion of Science for Young Scientist.

Notes and references

1 V. Biju, T. Itoh and M. Ishikawa, *Chem. Soc. Rev.*, 2010, **39**, 3031.
2 H. Kobayashi, M. Ogawa, R. Alford, P. L. Choyke and Y. Urano, *Chem. Rev.*, 2010, **110**, 2620.
3 A. Louie, *Chem. Rev.*, 2010, **110**, 3146.
4 X. Wu, X. He, K. Wang, C. Xie, B. Zhou and Z. Qing, *Nanoscale*, 2010, **2**, 2244.
5 K. Yong, I. Roy, W. Law and R. Hu, *Chem. Commun.*, 2010, **46**, 7136.
6 S. Taniguchi, M. Green, S. B. Rizvi and A. Seifalian, *J. Mater. Chem.*, 2011, **21**, 2877.
7 Y. T. Lim, S. Kim, A. Nakayama, N. E. Stott, M. G. Bawendi and J. V. Frangioni, *Mol. Imaging*, 2003, **2**, 50.
8 R. G. Aswathy, Y. Yoshida, T. Maekawa and D. S. Kumar, *Anal. Bioanal. Chem.*, 2010, **397**, 1417.
9 K. Soga, K. Tokuzen, K. Tsuji, T. Yamano, N. Venkatachalam, H. Hyodo and H. Kishimoto, *Proc. SPIE*, 2010, **7598**, 759807.
10 S. Sudo, *Optical Fiber Amplifiers: Materials, Devices, and Applications*, Artech House Publishers, Norwood, MA, 1997.
11 F. Wang, J. Wang and X. Liu, *Angew. Chem., Int. Ed.*, 2010, **49**, 7456.
12 T. Konishi, M. Shimizu, Y. Kameyama and K. Soga, *J. Mater. Sci.: Mater. Electron.*, 2007, **18**, 183.
13 D. Matsuura, *Appl. Phys. Lett.*, 2002, **81**, 4526.
14 D. Matsuura, T. Ikeuchi and K. Soga, *J. Lumin.*, 2008, **128**, 1267.
15 M. Kamimura, D. Miyamoto, Y. Saito, K. Soga and Y. Nagasaki, *Langmuir*, 2008, **24**, 8864.
16 J. Shen, L. Sun and C. Yan, *Dalton Trans.*, 2008, 5687.
17 F. Wang and X. Liu, *Chem. Soc. Rev.*, 2009, **38**, 976.
18 J. G. Bünzli, *Chem. Rev.*, 2010, **110**, 2729.
19 F. Wang, D. Banerjee, Y. Liu, X. Chen and X. Liu, *Analyst*, 2010, **135**, 1839.
20 H. S. Mader, P. Kele, S. M. Saleh and O. S. Wolfbeis, *Curr. Opin. Chem. Biol.*, 2010, **14**, 582.
21 C. Salthouse, S. Hildebrand, R. Weissleader and U. Mahmood, *Opt. Express*, 2008, **16**, 21731.
22 M. Nyk, R. Kumar, T. Y. Ohulchaskyy, E. J. Bergey and P. N. Prasad, *Nano Lett.*, 2008, **8**, 3834.
23 H. Kobayashi, N. Kosaka, M. Ogawa, N. Y. Morgan, P. D. Smith, C. B. Murray, X. Ye, J. Collins, A. Kumar, H. Bell and P. L. Choyke, *J. Mater. Chem.*, 2009, **19**, 6481.
24 S. A. Hilderbrand, F. Shao, C. Salthouse, U. Mahmood and R. Weissleder, *Chem. Commun.*, 2009, 4188.
25 Z. Wang, J. Hao, H. L. W. Chan, G. Law, W. Wong, K. Wong, M. B. Murphy, T. Su, Z. H. Zhang and S. Q. Zeng, *Nanoscale*, 2011, **3**, 2175.
26 H. Otsuka, Y. Nagasaki and K. Kataoka, *Adv. Drug Delivery Rev.*, 2003, **55**, 403.
27 Y. Nagasaki, *Chem. Lett.*, 2008, **37**, 564.
28 Y. Nagasaki, *Sci. Technol. Adv. Mater.*, 2010, **11**, 54505.
29 D. Miyamoto, M. Oishi, K. Kojima, K. Yoshimoto and Y. Nagasaki, *Langmuir*, 2008, **24**, 5010.
30 W. P. Wuelfing, S. M. Gross, D. T. Miles and R. W. Murray, *J. Am. Chem. Soc.*, 1998, **120**, 12696.
31 C. A. Traina and J. Schwartz, *Langmuir*, 2007, **23**, 9158.
32 C. A. Traina, T. J. Dennes and J. Schwartz, *Bioconjugate Chem.*, 2009, **20**, 437.
33 M. P. Danahy, M. J. Avaltroni, K. S. Midwood, J. E. Schwarzbauer and J. Schwartz, *Langmuir*, 2004, **20**, 5333.
34 F. Brodard-Severac, G. Guerrero, J. Maquet, P. Florian, C. Gervais and H. Muti, *Chem. Mater.*, 2008, **20**, 5191.
35 V. Zoulalian, S. Zurcher, S. Tosatti, M. Textor, S. Monge and J. Robin, *Langmuir*, 2010, **26**, 74.
36 H. B. Na, I. S. Lee, H. Seo, Y. I. Park, J. H. Lee, S. Kim and T. Hyeon, *Chem. Commun.*, 2007, 5167.
37 L. Qi, A. Sehgal, J. Castaing, J. Chapel, J. Fresnais, J. Berret and F. Cousin, *ACS Nano*, 2008, **2**, 879.
38 J. D. Goff, P. P. Huffstetler, W. C. Miles, N. Pothayee, C. M. Reinholz, S. Ball, R. M. Davis and J. S. Riffle, *Chem. Mater.*, 2009, **21**, 4784.
39 D. D. Perrin, W. L. F. Armarege and D. R. Perrin, *Purification of Laboratory Chemicals*, Pergamon, Oxford, 1980.
40 N. D. Scott, J. F. Walker and V. L. Hansley, *J. Am. Chem. Soc.*, 1936, **58**, 2442.
41 T. Yoshitomi, D. Miyamoto and Y. Nagasaki, *Biomacromolecules*, 2009, **10**, 596.
42 B. Boutevin, Y. Hervaud, A. Boulahna and E. M. E. Hadrami, *Polym. Int.*, 2002, **51**, 450.
43 C. E. Mckenna, M. T. Higa, N. H. Cheung and M. Mckenna, *Tetrahedron Lett.*, 1977, **2**, 155.
44 D. Avci and L. J. Mathias, *J. Polym. Sci., Part A: Polym. Chem.*, 2002, **40**, 3221.
45 N. Venkatachalam, Y. Saito and K. Soga, *J. Am. Ceram. Soc.*, 2009, **92**, 1006.
46 Y. Saito, K. Shimizu, M. Kamimura, H. Furusyo, K. Soga and Y. Nagasaki, *Trans. Mater. Res. Soc. Jpn.*, 2008, **33**, 803.